

ARTICLE

Received 27 Oct 2015 | Accepted 5 Jan 2016 | Published 4 Feb 2016

DOI: 10.1038/ncomms10622

OPEN

Cellular delivery and photochemical release of a caged inositol-pyrophosphate induces PH-domain translocation *in cellulo*

Igor Pavlovic¹, Divyeshsinh T. Thakor¹, Jessica R. Vargas², Colin J. McKinlay², Sebastian Hauke³, Philipp Anstaett¹, Rafael C. Camuña⁴, Laurent Bigler¹, Gilles Gasser¹, Carsten Schultz³, Paul A. Wender² & Henning J. Jessen⁵

Inositol pyrophosphates, such as diphospho-myo-inositol pentakisphosphates (InsP₇), are an important family of signalling molecules, implicated in many cellular processes and therapeutic indications including insulin secretion, glucose homeostasis and weight gain. To understand their cellular functions, chemical tools such as photocaged analogues for their real-time modulation in cells are required. Here we describe a concise, modular synthesis of InsP₇ and caged InsP₇. The caged molecule is stable and releases InsP₇ only on irradiation. While photocaged InsP₇ does not enter cells, its cellular uptake is achieved using nanoparticles formed by association with a guanidinium-rich molecular transporter. This novel synthesis and unprecedented polyphosphate delivery strategy enable the first studies required to understand InsP₇ signalling in cells with controlled spatiotemporal resolution. It is shown herein that cytoplasmic photouncaging of InsP₇ leads to translocation of the PH-domain of Akt, an important signalling-node kinase involved in glucose homeostasis, from the membrane into the cytoplasm.

¹Department of Chemistry, University of Zurich, Winterthurerstrasse 190, Zurich 8057, Switzerland. ²Departments of Chemistry and Chemical and Systems Biology, Stanford University, Stanford, California 94305, USA. ³European Molecular Biology Laboratory (EMBL), Cell Biology & Biophysics Unit, Meyerhofstrasse 1, 69117 Heidelberg, Germany. ⁴Departamento de Química Orgánica, Facultad de Ciencias, Universidad de Málaga, Malaga 29071, Spain. ⁵Department of Chemistry and Pharmacy, Albert-Ludwigs University Freiburg, Albertstrasse 21, 79104 Freiburg, Germany. Correspondence and requests for materials should be addressed to P.A.W. (email: Wenderp@stanford.edu) or to H.J.J. (email: henning.jessen@oc.uni-freiburg.de).

Diphospho-inositol polyphosphates (InsP₇) are second messengers involved in essential cell signalling pathways^{1–4}. A distinct difference of InsP₇ compared with other inositol polyphosphates is the presence of a phosphoanhydride bond in, for example, the 5-position (5-InsP₇, Fig. 1), rendering them a structurally unique class of second messengers. This special feature is also the reason for their nickname ‘inositol pyrophosphates’. InsP₇ are implicated in the regulation of diverse cellular and metabolic functions in different kingdoms of life^{1–8}. It has been proposed that InsP₇ bind to the pleckstrin homology (PH) domain of protein kinase B (Akt), and competitively suppress its specific phosphatidylinositol 3,4,5-trisphosphate (PIP₃) association at the plasma membrane, thereby inhibiting phosphoinositide-dependent kinase 1 (PDK1)-mediated phosphorylation of Akt^{9,10}. However, there remains uncertainty as to whether the reduced phosphorylation of Akt is a result of the inhibition of its membrane association via its PH-domain, since the *in vitro* assays that have been performed do not contain any membrane or membrane mimics. In addition, InsP₇ might act either as allosteric inhibitors or as non-enzymatic phosphorylating agents or both^{3,11}. Notwithstanding, inhibition of the Akt pathway by InsP₇ has an impact on glucose uptake and insulin sensitivity, as exemplified by a mouse model that lacks inositol hexakisphosphate-kinase 1 (IP6K1). These knockout mice have reduced levels of InsP₇ and show a lean phenotype on high-fat diet concomitant with increased insulin sensitivity⁹. As a consequence, IP6K1 has recently been proposed as a novel target in the treatment of diabetes and obesity¹². To address fundamental questions about the mechanism of action of these potent signalling molecules and their subcellular localization, the development of new chemical tools is required.

To understand cellular signalling mediated by second messengers, photocaged analogues that can be activated on demand inside living cells with spatiotemporal resolution have attracted great interest¹³. Unfortunately, preparation of such analogues often requires lengthy synthetic sequences. Phosphorylated second messengers derived from *myo*-inositol such as *myo*-inositol 1,4,5-trisphosphate (Fig. 1) present additional challenges as their polyanionic nature precludes efficient cellular uptake¹⁴. For example, while cell-permeable and photocaged analogues of different *myo*-inositol polyphosphates (InsP_x) and phosphatidyl *myo*-inositol polyphosphates (PtdIns-P_x) have been reported^{15–18}, the phosphate groups typically need to be reversibly masked. This complicates their use, as multiple intracellular hydrolysis events must occur before the free polyphosphate is formed¹⁹. Even so, no such photocaged derivatives are currently available for the more complex

diphospho-*myo*-inositol pentakisphosphates as, for example, 5-InsP₇ (Fig. 1)²⁰.

Here we report the design, step-economical synthesis, photophysical and metabolic evaluation of photocaged 5-InsP₇, and significantly, a general solution to the delivery of unmodified polyphosphate probes into cells using guanidinium-rich molecular transporters²¹. On cytoplasmic uncaging, 5-InsP₇-mediated PH-domain translocation from the membrane into the cytosol in living cells is demonstrated for the first time on a 15-min timescale.

Results

Synthesis. All current synthetic approaches to access any InsP₇ isomer rely on a global hydrogenation in the last step, during which up to 13 protecting groups need to be removed^{22–30}. Significantly, however, hydrogenation is incompatible with photocaging groups and many other functional moieties like, for example, fluorophores. To address this problem, a novel strategy based on the development of a levulinate benzyl ester adaptor (LevB) is described. The introduction of this new protecting group and its combination with fluorenylmethyl (Fm) protection^{31–33} and photocage introduction enables the previously inaccessible synthesis of the first photoactivatable diphospho-inositol InsP₇ probe **9** equipped with a [7-(diethylamino)-coumarin-4-yl]methyl (DEACM) photocage (Fig. 2a). It is noteworthy that this strategy potentially facilitates the introduction of other tags, such as, for example, photoaffinity labels and fluorophores.

The synthesis commenced with benzylidene protected **2** prepared as previously described (Fig. 2a)²³. The 5-OH position of **2** is available for phosphorylation, allowing virtually any protected phosphate to be introduced. However, none of the existing protecting groups are compatible with the subsequent introduction of the coumarin cage. Such protecting groups would need to be stable under acidic and basic conditions and must enable double deprotection under very mild conditions. To meet these stringent requirements, a new phosphate-protecting group is required. The approach described herein is based on an Umpolung strategy that had been exploited in prodrug design for nucleotides^{34,35}. Conceptually, this strategy is useful to generally couple phenol or alcohol protecting groups to phosphates via a benzyl adaptor, greatly enhancing the available protecting group strategies for phosphates (Fig. 2b). A novel P-amidite **3** was developed (Fig. 2, Supplementary Fig. 1), which is connected via a benzyl ester to a levulinate group (LevB). After oxidation to the phosphate triester **6**, the LevB group can be cleaved by hydrazone formation, initiating cyclization and finally a Grob-type fragmentation to give the unprotected phosphates (Fig. 2b).

After coupling P-amidite **3** to alcohol **2** and oxidation, all inositol-protecting groups were cleaved with TFA. The resultant protected monophosphate **4** was phosphorylated with (Fm)₂-P-amidite **5** and oxidized. Notwithstanding the significant molecular crowding of hexakisphosphate **6**, both LevB groups were efficiently cleaved under mild conditions (hydrazine*AcOH/TFA), releasing phosphate **7**. Next, the P-anhydride was formed using Fm-protected photocaged P-amidite **8** (ref. 33). All 11 Fm-protecting groups were then cleaved with piperidine resulting in highly pure photocaged 5-InsP₇ **9** in 45% yield over 2 steps (11% overall yield from **1**) on precipitation of the compound as the dodeca-piperidinium salt. The piperidinium ions can also be exchanged with sodium ions by precipitation. In addition, natural 5-InsP₇ **10** can be prepared following the same strategy by using (Fm)₂-P-amidite **5** in the anhydride forming reaction (8% overall yield from **1**)^{36,37}. This eight-step synthesis represents a general strategy to access 5-InsP₇ **10** and caged analogues in scalable amounts (30 mg of **9** have been prepared) and very high quality

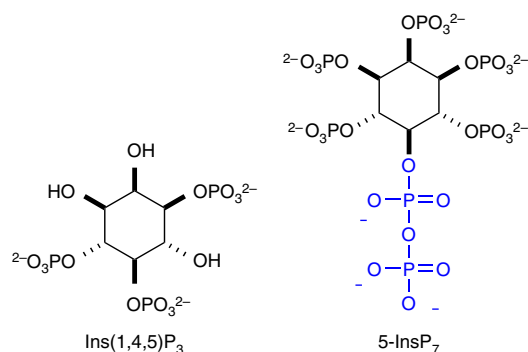


Figure 1 | Phosphorylated second messengers derived from *myo*-inositol. Chemical structures of *myo*-inositol 1,4,5-trisphosphate and 5-diphospho-*myo*-inositol pentakisphosphate (5-InsP₇).

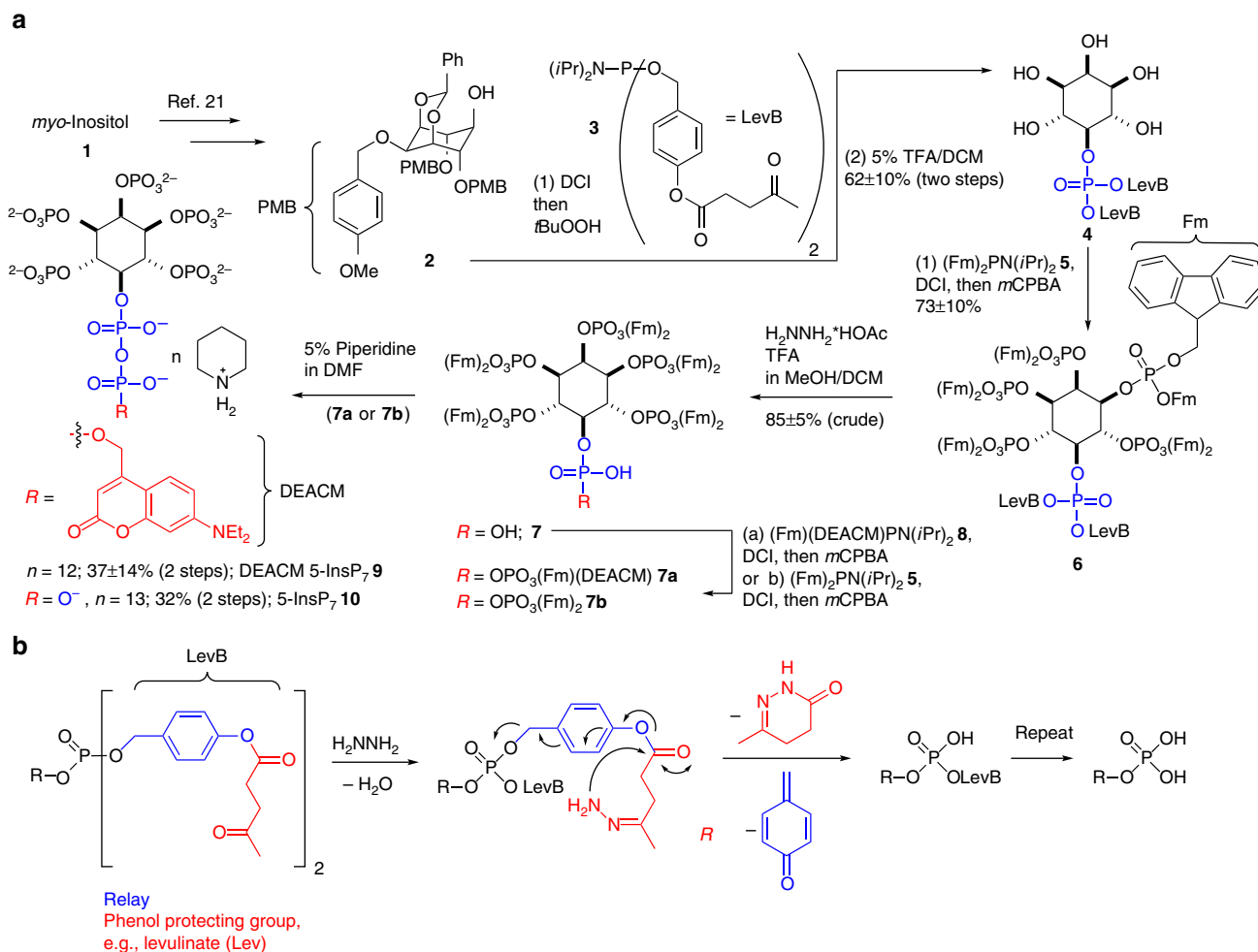


Figure 2 | Synthesis of photocaged 5-InsP₇ and mechanism of LevB cleavage. (a) Synthesis of DEACM 5-InsP₇ **9** and 5-InsP₇ **10** based on fluorenylmethyl (Fm) protection and a novel phosphate-protecting group (LevB). DCI, 4,5-dicyanoimidazole; DEACM, [7-(diethylamino)-coumarin-4-yl]methyl; Fm, fluorenylmethyl; *m*CPBA, metachloro perbenzoic acid; TFA, trifluoroacetic acid. (b) An adaptor strategy for phosphate release: hydrazine triggers levulinate (red) cleavage and 1,6-elimination (blue) to release free phosphate. Generally, levulinate could also be replaced with other phenol protecting groups.

without the need for a final hydrogenation under aqueous conditions.

In vitro stability and photophysical properties. To serve as a useful tool, DEACM 5-InsP₇ **9** must be stable towards enzymatic digestion to enable cellular uptake and release only on photolysis. To test its stability, **9** was incubated in tissue homogenate (brain, Fig. 3a; liver, Supplementary Fig. 3 and Supplementary Methods) and cell extract (Supplementary Figs 4–5 and Supplementary Methods). Readout was achieved by resolution on polyacrylamide gels (35%, Fig. 3 and Supplementary Methods)³⁸. DEACM 5-InsP₇ **9** did not decompose under these conditions over incubation times up to 5 h (Fig. 3a, Lanes III–V and Supplementary Figs 3–5). Thus, **9** is a probe that has the potential to be broadly applied in different cell and tissue types. Importantly, on exposure to ultraviolet light (366 nm, 4 W, distance 10 cm) in extracts, it was cleanly converted into 5-InsP₇ **10**, as verified by PAGE (Fig. 3a, Lanes VI and VII and Supplementary Figs 3–4) and HPLC analysis (Supplementary Fig. 6) with **10** as a standard.

Next, the photophysical properties of DEACM 5-InsP₇ **9** were characterized. The quantum yield for the disappearance of **9** $\Delta\phi_{chem}$ is 0.71% at 355 nm as determined by actinometry following a novel protocol (Supplementary Methods)^{39–41}. The

fluorescence quantum yield ϕ_f is 6.2% and the lifetime τ_f is 1.2 ns. Notably, **9** also exhibits typical coumarin fluorescence at 500 nm (excitation at 386 nm; Supplementary Figs 7–10 and Supplementary Methods)^{33,42}.

Cellular delivery and uncaging. Notwithstanding the efficiency of this synthesis, it was found as expected that DEACM 5-InsP₇ **9**, like other polyanions^{11,14}, does not readily cross the non-polar membrane of a cell (Fig. 4b,c). To address this problem, its non-covalent complexation, cell uptake and release using guanidinium-rich molecular transporters were studied⁴³. **9** was mixed with amphipathic, guanidinium-rich transporter **11** (Fig. 4a), in an equimolar ratio to form nanoparticles. HeLa cells were treated with these complexes and analysed for coumarin fluorescence by flow cytometry. Significantly, while DEACM 5-InsP₇ **9** itself does not appreciably enter cells, the transporter-complexed **9** does, as demonstrated by a 10-fold increase in intracellular fluorescence (Fig. 4b). According to flow cytometry analysis, over 99% of cells display increased levels of **9** following treatment with the transporter/DEACM-InsP₇ complex (Fig. 4c). It is important to note that other transfection reagents like Lipofectamine 2000 do not efficiently deliver **9** into cells (Fig. 4b).

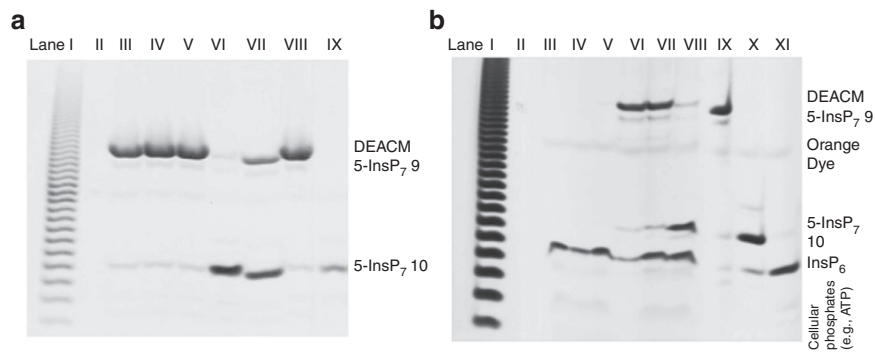


Figure 3 | *In vitro* and *in cellulo* release of 5-InsP₇. (a) Analysis of DEACM 5-InsP₇ **9** by gel electrophoresis (PAGE) and toluidine blue staining. **9** is stable for hours in rat brain extract (lanes III–V) and can be uncaged by ultraviolet irradiation (lane VI). Lane I: poly-P marker. Lane II: empty. Lane III: **9** in brain extract (3 h). Lane IV: **9** in brain extract (2 h). Lane V: **9** in brain extract (1 h). Lane VI: **9** in brain extract (1 h), then ultraviolet irradiation (15 min). Lane VII: **9** in distilled water, then ultraviolet irradiation (15 min). Lane VIII: **9**. Lane IX: 5-InsP₇ **10**. (b) Analysis of cellular uptake and *in cellulo* photouncaging with and without MoTr **11** after TiO₂ microsphere extraction followed by gel electrophoresis (PAGE). Bands containing **9** and **10** were additionally extracted and analysed by MALDI mass spectrometry. **9** only enters cells in the presence of MoTr **11** (lanes VI, VII) and can be uncaged in living cells (lane VIII). Lane I: Poly-P marker to assess quality of separation. Lane II: empty. Lane III: HeLa cells (control). Lane IV: HeLa cells + **11** (control). Lane V: HeLa cells + **9** (5 h). Lane VI: HeLa cells + **9** + **11** (5 h), Lane VII: HeLa cells + **9** + **11** (16 h). Lane VIII: HeLa cells + **9** + **11** (16 h, then 10 min irradiation 366 nm, 4W). Lane IX: DEACM 5-InsP₇ **9** (control). Lane X: 5-InsP₇ **10** (control). Lane XI: InsP₆ (control).

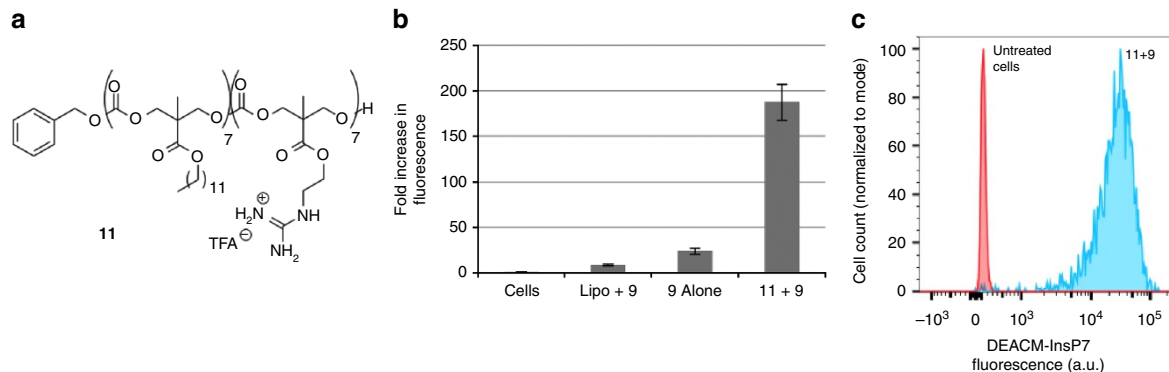


Figure 4 | Intracellular delivery of photocaged 5-InsP₇ to HeLa cells with a guanidinium-rich transporter. (a) Structure of amphipathic oligocarbonate transporter, **11**. (b) Cellular uptake of **9** as determined by flow cytometry. Complexes were formulated at a 1:1 mole ratio of **9** (5 μM) to **11**. Values reported are normalized to the autofluorescence of untreated cells. (c) Histogram plot of intracellular fluorescence demonstrates >99% delivery efficiency to cells.

Delivery and intracellular distribution of **9** were further analysed in HeLa cells by confocal microscopy after 4 and 16 h (Fig. 5). The z-stack analysis shows DEACM 5-InsP₇ **9** distributed throughout the cytoplasm at both time points (Fig. 5, single z-slice shown). Both diffuse fluorescence and fluorescent puncta are observed, consistent with mixed diffusion or endosomal uptake and release^{44–46}. This is additionally supported by a 65% reduction in cellular uptake when cells were treated at 4 °C, a condition known to inhibit most endocytotic processes (Supplementary Fig. 11).

Cellular uptake, stability and efficient uncaging in living cells was additionally verified by extraction of diphospho-inositol polyphosphates and other cellular phosphates based on a recently published TiO₂ microsphere enrichment method⁴⁷. Here it is shown that this method can also be used to extract analogues such as **9** from complex cell and tissue lysates (Fig. 3b and Supplementary Methods) enabling studies concerning its intracellular fate after delivery. After incubation of DEACM 5-InsP₇ **9** with HeLa cells in the presence or absence of MoTr **11** and repeated washings to remove external **9**, the extracts prepared from those cells (1 million cells) clearly showed a distinct novel band corresponding to **9** in the PAGE analysis after enrichment with TiO₂ and elution (Fig. 3b, lanes VI–VII), whereas no such

uptake could be detected in the control experiment without transporter (Fig. 3b, lane V). To verify its identity, the band corresponding to DEACM 5-InsP₇ **9** was extracted from the gel and analysed by MALDI mass spectrometry, demonstrating its intracellular stability (Supplementary Fig. 12 and Supplementary Methods) for multiple hours. Moreover, efficient intracellular uncaging by irradiation at 366 nm was proven using the same extraction and resolution method (TiO₂ enrichment, then PAGE) in combination with mass spectrometry after extraction of Lane VIII (Fig. 3b). These conditions were found to be of no immediate toxicity (Supplementary Fig. 13 and Supplementary Methods). In summary, the photocaged molecule **9** is efficiently taken up by cells in the presence of MoTr **11**, evenly distributed throughout the cytoplasm, stable for multiple hours in its caged form and can be selectively uncaged to 5-InsP₇ **10**, thus fulfilling the stringent requirements imposed on an intracellular signalling probe.

PH-domain translocation. To determine the suitability of the combined delivery and uncaging strategy for a deeper understanding of the effect of InsP₇ fluctuations, PH-domain translocation on cytoplasmic InsP₇ release was studied. The rationale for this experiment is provided by the lean phenotype displayed by IP6K1 knockout mice on high-fat diet and the observation that

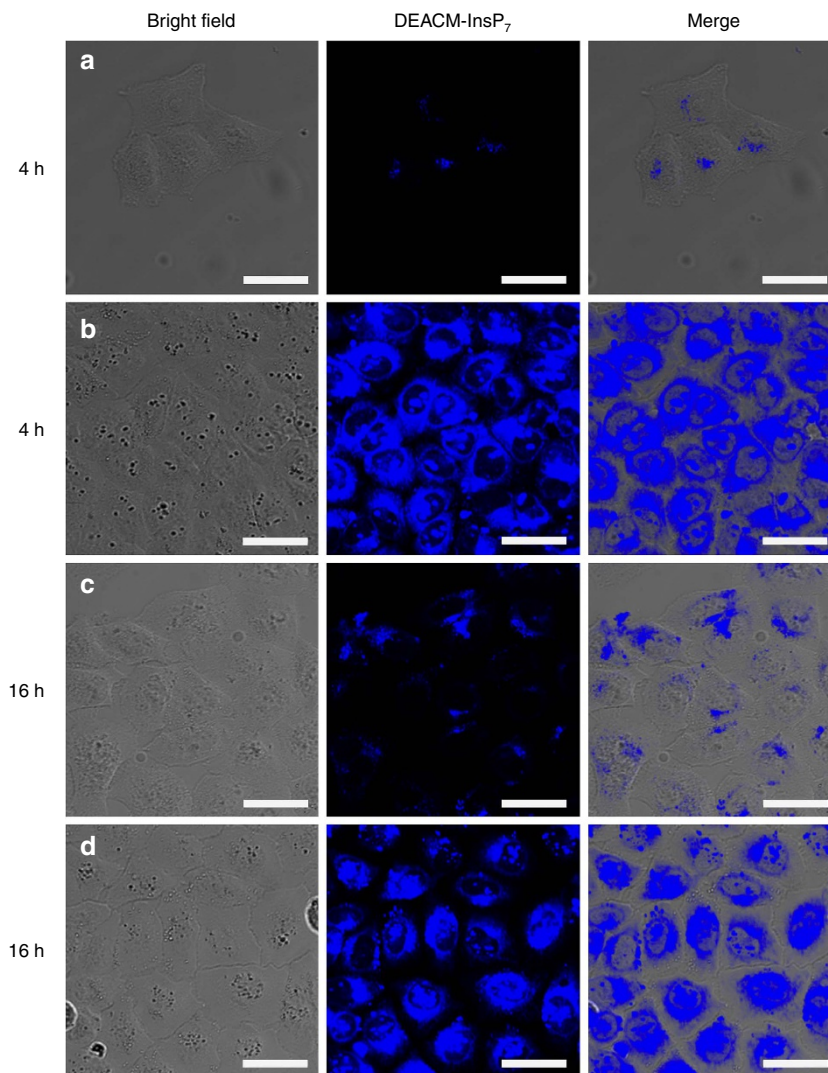


Figure 5 | The molecular transporter 11 delivers photocaged 5-InsP₇ into the cytoplasm. Confocal microscopy analysis of HeLa cells incubated with 5 μ M DEACM-InsP₇ **9** in the presence or absence of transporter **11** after 4 and 16 h of incubation. Efficient uptake of **9** is demonstrated by blue coumarin fluorescence emitted from the compound. Cells treated with (a) **9** alone for 4 h, (b) **9** + **11** for 4 h, (c) **9** alone for 16 h and (d) **9** + **11** for 16 h. Scale bars, 35 μ m.

InsP₇ inhibit Akt phosphorylation *in vitro* and *in vivo* by binding to the PH-domain⁹. Collectively, these findings suggest an effect of 5-InsP₇ on membrane localization of Akt. However, no tool to augment any InsP₇ within seconds in living cells was previously available. With the new tools in hand, HeLa cells were transiently transfected with a plasmid expressing the PH-domain of Akt fused to an enhanced green fluorescent reporter protein (eGFP)^{48,49}. Cells were serum-starved to induce cytoplasmic localization of the PH-domain due to absence of growth factors and therefore inactivation of the PI3K/Akt/mTOR pathway⁵⁰. PH-eGFP plasma membrane association was then efficiently induced within 10 min on external addition of a combination of growth factors (insulin-like growth factor (IGF); endothelial growth factor (EGF)) into the medium. During the starvation period, cells were loaded with caged InsP₇ **9**/MoTr **11** nanoparticles for 4 h. This treatment alone had no effect on PH-domain localization. Next, cells were irradiated under a confocal laser-scanning microscope with short laser pulses (375 nm, 10 MHz, 30 s) in different areas (Fig. 6 dotted circle, and Supplementary Figs 14–23), and PH-domain localization was traced using the green channel. After photouncaging, a delayed

but complete PH-domain translocation from the plasma membrane into the cytoplasm was observed, and these results were repeated several times ($n=4$). Significantly, translocation did not occur when cells were incubated with photocaged InsP₇ **9** or MoTr **11** only (Supplementary Figs 18–23). In these cases, the PH-domains remained localized on the membrane for several hours, demonstrating the need for the presence of all components and ruling out photobleaching of eGFP in the irradiated areas. A detailed analysis of additional micrographs in pseudo-colour with ratiometric changes is shown in the Supplementary Information (Supplementary Figs 14–23). This is the first example of controlled 5-InsP₇ **10** augmentation inside of a living cell within a few seconds timeframe coupled to a microscopic readout on the single cell level. We posit that this strategy will be useful to understand InsP₇ signalling in more detail as previously possible, as evidenced by the delayed PH-domain translocation observed for the first time in our experiments.

Discussion

This study provides a new strategy to synthesize InsP₇ that enables introduction of caging subunits. The potential utility of

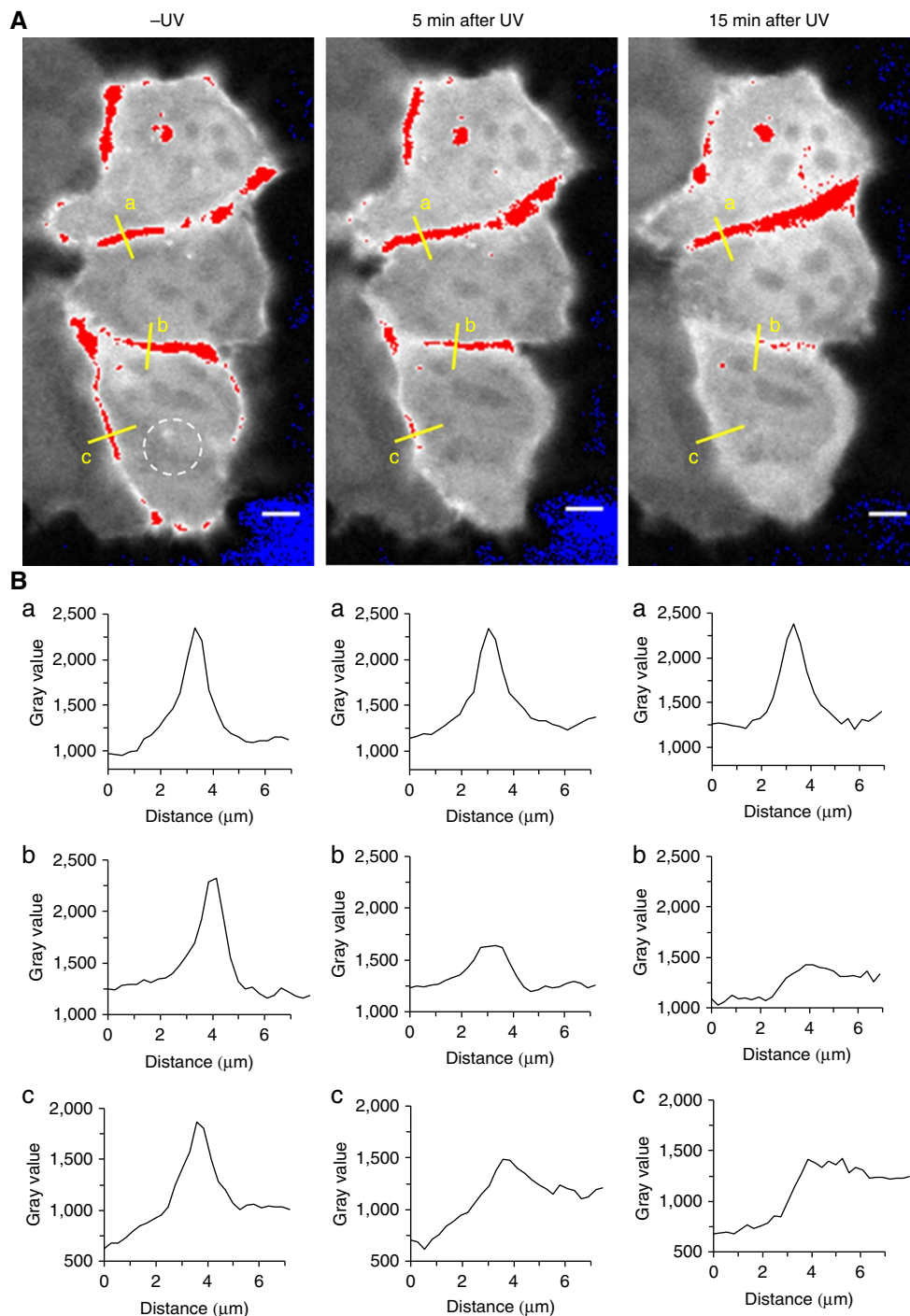


Figure 6 | PH-domain translocation in irradiated and control cells. Confocal fluorescence microscopy analysis of PH-eGFP translocation in HeLa Kyoto cells after photouncovering in defined areas (dotted circle). **(A)** Serum-starved cells were loaded with $5\ \mu\text{M}$ **9** + **11** for 4 h and then stimulated with IGF and EGF ($100\ \text{ng ml}^{-1}$). Robust recruitment of the PH-domain to the membrane is observed. Photouncovering in the dotted area (white circle) is achieved by short ultraviolet laser pulses and the change of fluorescence intensity followed over time (0, 5 and 15 min). **(B)** Development of the fluorescence intensity (indicated as gray value) over time (0, 5, 15 min) in three different membrane sections (a, b, c; distance in μm). Photouncovering leads to translocation of the PH-eGFP construct into the cytoplasm after 5 min from the membrane of the irradiated cell. After 15 min, complete translocation of the PH-domain into the cytoplasm is observed (**B**, b and c), whereas in the non-irradiated control cell the PH-eGFP construct remains localized on the membrane (**B**, a). Images are presented in pseudo-colour, normalized over time. Intensities were acquired pre-saturated, with the entire dynamic range of intensity available. Scale bars, $5\ \mu\text{M}$.

photocaged 5-InsP₇ **9** was demonstrated by photon-triggered uncaging in rat brain homogenate and other cell extracts. A complex of **9** with molecular transporter **11** was then shown to efficiently enter cells after non-covalent nanoparticle assembly.

Collectively, these results provide the first example of the synthesis of a photocaged analogue of InsP₇ and of its subsequent delivery into cells using non-covalent complexation with a guanidinium-rich molecular transporter. A recently developed

TiO₂ microsphere enrichment method was applied to study the *in cellulo* stability of 5-InsP₇ analogues and their efficient photochemical release in combination with MALDI mass spectrometry. We expect that this combined synthesis, delivery and analytical strategy will find widespread and general application in cell signalling studies as a convenient way to rapidly augment 5-InsP₇ **10** with spatiotemporal resolution. Along these lines, it was shown that cytoplasmic release of 5-InsP₇ triggers delayed but complete membrane desorption of the PH-domain of Akt within 15 min. In the human proteome, PH-domains are the 11th most common domain⁵¹, and the new approach described in this publication will enable a systematic understanding of the effect of inositol-pyrophosphate augmentation on protein localization.

Methods

Experimental data of synthetic compounds. For ¹H, ¹³C and ³¹P NMR spectra of compounds and MALDI and HR-ESI MS spectra see Supplementary Figs 24–70. ¹H NMR spectra were recorded on Bruker 400 MHz spectrometers or Bruker 500 MHz spectrometers (equipped with a cryo platform) at 298 K in the indicated deuterated solvent. ³¹P [¹H]-NMR spectra and ³¹P NMR spectra were recorded with ¹H-decoupling or ¹H coupling on Bruker 162 MHz or Bruker 202 MHz spectrometers (equipped with a cryo platform) at 298 K in the indicated deuterated solvent. All signals were referenced to an internal standard (PPP). ¹³C [¹H]-NMR spectra were recorded with ¹H-decoupling on Bruker 101 MHz or Bruker 125 MHz spectrometers (equipped with a cryo platform) at 298 K in the indicated deuterated solvent. All signals were referenced to the internal solvent signal as standard (CDCl₃, δ 77.0; CD₃OD, δ 49.0; DMSO-d₆, δ 39.5).

Detailed synthetic procedures for all new compounds are provided in the Supplementary Information (see Supplementary Methods, chemical synthesis).

Cellular uptake by flow cytometry. Caged-IP7 **9** and oligomer **11** were brought up in pH 7.4 PBS buffer at 1 mM concentrations. HeLa cells were seeded at 40,000 cells per well in a 24-well plate and allowed to adhere overnight. The IP7:co-oligomer complexes were formed at a 1:1 molar ratio by mixing 8 μl of 1 mM oligomer stock with 8 μl of 1 mM caged-IP7 **9** stock in 184 μl PBS pH 7.4. For conditions with caged-IP7 **9** alone, 8 μl of 1 mM caged-IP7 **9** stock was added to 192 μl PBS pH 7.4. The complexes were allowed to incubate for 30 min at room temperature. The Lipofectamine 2000 control was prepared in OptiMEM according to the manufacturer's instructions (0.75 μl Lipofectamine into 62.5 μl OptiMEM, 8 μl caged-IP7 **9** stock into 54.5 μl OptiMEM). The cells were washed with ~0.5 ml serum-free DMEM medium, then 400 μl serum-free DMEM was added to wells with untreated cells; 368.75 μl to wells treated with Lipofectamine 2000; 350 μl to treated wells. Then 31.25 μl Lipofectamine:caged-IP7 **9** and 50 μl of the caged-IP7:co-oligomer complexes were added to each respective well for a final caged-IP7 **9** concentration of 5 μM; all conditions were performed in triplicate. The cells were incubated at 37 °C for 3 h. The medium was then removed and the cells were washed with 1.0 ml PBS. About 0.4 ml EDTA trypsin was added, and the cells incubated for 8 min at 37 °C. Next, 0.6 ml of serum-containing DMEM medium was added, and the contents of each well were transferred to a 15 ml centrifuge tube and centrifuged (1,200 r.p.m. for 5 min). The cells were collected and re-dispersed in 200 μl PBS, transferred to FACS tubes, and read on a flow cytometry analyser. Results were analysed using FlowJo software. The data presented are the mean fluorescent signals from 10,000 cells analysed.

Fluorescence microscopy. Confocal microscopy was conducted on a CLSM SP5 Mid ultraviolet–visible Leica inverted confocal laser-scanning microscope equipped with a 15 W MaiTai DeepSee twophoton laser (Stanford Cell Sciences Imaging Facility, Award #S10RR02557401 from the National Center for Research Resources). HeLa cells were incubated in serum-free DMEM with 5 μM **9** or **11** (equimolar), for 4 or 16 h. After incubation, media was removed and cells washed 3 × with 1.0 mg ml⁻¹ heparin (180 U mg⁻¹, Aldrich) solution in PBS, then imaged in clear serum-free DMEM. Pictures were recorded with a HCX APO L × 20/1.00 water immersion objective and photomultiplier tube detector.

eGFP-Akt-PH-domain translocation. Mammalian cells (HeLa Kyoto) were grown up to 50–60% confluence (eight wells Lab-Tek Chamber Slide) in 250 μl DMEM (10% FBS, 10% Pen/Strep, high glucose (4.5 g l⁻¹)) at 37 °C, 5% CO₂ for 16 h. Cells were then washed with 250 μl PBS followed by a wash with serum-free DMEM (-FBS, -Pen/Step). About 230 μl serum-free DMEM medium were then added to each well.

Transfection of HELA cells with the eGFP Akt-PH-domain for imaging: The transfection mixture was prepared for eight wells. About 200 ng DNA (eGFP-Akt-PH) in 150 μl DMEM (-FBS) were incubated for 10 min at room temperature. Then, 10 μl FuGENE transfecting reagent were added to DNA

containing DMEM (-FBS) medium and incubated for 20 min at room temperature. About 20 μl of the transfection mixture were then added to each well. Cells were incubated for 6–8 h at 37 °C (5% CO₂). After this period, the transfection mixture was removed by washing the cells with 250 μl PBS and DMEM (-FBS). Cells were starved by adding 250 μl DMEM (-FBS) and incubated for 14–16 h at 37 °C (5% CO₂).

After overnight starvation, the cells were washed with PBS (250 μl) and 230 μl DMEM (-FBS) were added. Afterwards, 20 μl sample mixture (consisting of caged InsP₇:Co-oligomer (D:G7:7) complexes) were added to each well and distributed equally. The final concentration of the complex was 5 μM for each well. Cells were then incubated at 37 °C (5% CO₂) for 4 h.

Imaging of Akt-PH translocation. After 4-h incubation with **9** and **11**, HeLa cells were washed with 250 μl (2 ×) imaging buffer (115 mM NaCl, 1.2 mM CaCl₂, 1.2 mM MgCl₂, 1.2 mM K₂HPO₄, 20 mM HEPES). About 200 μl imaging buffer were added to the wells. Translocation of eGFP-Akt-PH to the membrane was stimulated by adding a mixture of growth factors EGF and IGF (100 ng ml⁻¹ each). Translocation was monitored over 10 min at 37 °C (5% CO₂).

Cells that had responded to treatment with the growth factors and that had the PH-domain localized at the membrane were used in the uncaging experiments by confocal laser-scanning microscopy. Non-illuminated neighboring cells were used as controls.

Confocal laser-scanning microscopy. Imaging was performed on an Olympus IX83 confocal laser-scanning microscope at 37 °C in a 5% CO₂ high humidity atmosphere (EMBL incubation box). Imaging was performed using an Olympus Plan-APON × 60 (numerical aperture 1.4, oil) objective. The images were acquired utilizing a Hamamatsu C9100-50 EM CCD camera. Image acquisition was performed via FluoView imaging software, version 4.2. The green channel was imaged using the 488 nm laser line (120 mW cm⁻²) at 3% laser power and a 525/50 emission mirror. The red channel was imaged using the 559 nm laser (120 mW cm⁻²) at 2.0% laser power and a 643/50 emission filter. A pulsed 375 nm laser line (10 MHz) was applied for uncaging experiments. For uncaging experiments, circular regions of interest of 4–10 μm diameter were pre-defined. Pre-activation images were captured for five frames (5 s per frame), followed by 30 s of activation within the regions of interest. Recovery images were captured for 35 min at a frame rate of 5 s per frame.

Image analysis. Image analysis was conducted utilizing Fiji open source image analysis software tool⁵². Lookup tables were applied to match the colour within the recorded image with the wavelengths of detected light. For comparability, the lookup tables of pre- and postactivated images were set the same weighting.

References

- Bennett, M., Onnebo, S. M. N., Azevedo, C. & Saiardi, A. Inositol pyrophosphates: metabolism and signalling. *Cell. Mol. Life Sci.* **63**, 552–564 (2006).
- Monserrate, J. P. & York, J. D. Inositol phosphate synthesis and the nuclear processes they affect. *Curr. Opin. Cell Biol.* **22**, 365–373 (2010).
- Shears, S. B., Weaver, J. D. & Wang, H. Structural insight into inositol pyrophosphate turnover. *Adv. Biol. Regul.* **53**, 19–27 (2013).
- Wilson, M. S. C., Livermore, T. M. & Saiardi, A. Inositol pyrophosphates: between signalling and metabolism. *Biochem. J.* **452**, 369–379 (2013).
- Rao, F. *et al.* Inositol pyrophosphates promote tumor growth and metastasis by antagonizing liver kinase B1. *Proc. Natl Acad. Sci. USA* **112**, 1773–1778 (2015).
- Rao, F. *et al.* Inositol hexakisphosphate kinase-1 mediates assembly/disassembly of the CRL4-signalosome complex to regulate DNA repair and cell death. *Proc. Natl Acad. Sci. USA* **111**, 16005–16010 (2014).
- Laha, D. *et al.* VIH2 regulates the synthesis of inositol pyrophosphate InsP8 and jasmonate-dependent defenses in Arabidopsis. *Plant Cell* **27**, 1082–1097 (2015).
- Illies, C. *et al.* Requirement of inositol pyrophosphates for full exocytotic capacity in pancreatic beta cells. *Science* **318**, 1299–1302 (2007).
- Chakraborty, A. *et al.* Inositol pyrophosphates inhibit akt signalling, thereby regulating insulin sensitivity and weight gain. *Cell* **143**, 897–910 (2010).
- Luo, H. R. *et al.* Inositol pyrophosphates mediate chemotaxis in dictyostelium via pleckstrin homology domain-PtdIns(3,4,5)P₃ interactions. *Cell* **114**, 559–572 (2003).
- Wu, M. X. *et al.* Elucidating diphosphoinositol polyphosphate function with nonhydrolyzable analogues. *Angew. Chem. Int. Ed.* **53**, 7192–7197 (2014).
- Mackenzie, R. W. & Elliott, B. T. Akt/PKB activation and insulin signalling: a novel insulin signalling pathway in the treatment of type 2 diabetes. *Diabetes Metab. Syndr. Obes.* **7**, 55–64 (2014).
- Yu, H. T., Li, J. B., Wu, D. D., Qiu, Z. J. & Zhang, Y. Chemistry and biological applications of photo-labile organic molecules. *Chem. Soc. Rev.* **39**, 464–473 (2010).

14. Ozaki, S., DeWald, D. B., Shope, J. C., Chen, J. & Prestwich, G. D. Intracellular delivery of phosphoinositides and inositol phosphates using polyamine carriers. *Proc. Natl Acad. Sci. USA* **97**, 11286–11291 (2000).
15. Best, M. D., Zhang, H. L. & Prestwich, G. D. Inositol polyphosphates, diphosphoinositol polyphosphates and phosphatidylinositol polyphosphate lipids: Structure, synthesis, and development of probes for studying biological activity. *Nat. Prod. Rep.* **27**, 1403–1430 (2010).
16. Hoglinger, D., Nadler, A. & Schultz, C. Caged lipids as tools for investigating cellular signalling. *Biochim. Biophys. Acta* **1841**, 1085–1096 (2014).
17. Kantevari, S., Gordon, G. R. J., MacVicar, B. A. & Ellis-Davies, G. C. R. A practical guide to the synthesis and use of membrane-permeant acetoxyethyl esters of caged inositol polyphosphates. *Nat. Protoc.* **6**, 327–337 (2011).
18. Li, W. H., Llopis, J., Whitney, M., Zlokarnik, G. & Tsien, R. Y. Cell-permeant caged InsP(3) ester shows that Ca^{2+} spike frequency can optimize gene expression. *Nature* **392**, 936–941 (1998).
19. Pavlovic, I. *et al.* Prometabolites of 5-Diphospho-myo-inositol Pentakisphosphate. *Angew. Chem. Int. Ed.* **54**, 9622–9626 (2015).
20. Glennon, M. C. & Shears, S. B. Turnover of inositol pentakisphosphates, inositol hexakisphosphate and diphosphoinositol polyphosphates in primary cultured-hepatocytes. *Biochem. J.* **293**, 583–590 (1993).
21. Geihe, E. I. *et al.* Designed guanidinium-rich amphipathic oligocarbonate molecular transporters complex, deliver and release siRNA in cells. *Proc. Natl Acad. Sci. USA* **109**, 13171–13176 (2012).
22. Albert, C. *et al.* Biological variability in the structures of diphosphoinositol polyphosphates in Dictyostelium discoideum and mammalian cells. *Biochem. J.* **327**, 553–560 (1997).
23. Capolicchio, S., Thakor, D. T., Linden, A. & Jessen, H. J. Synthesis of unsymmetric diphospho-inositol polyphosphates. *Angew. Chem. Int. Ed.* **52**, 6912–6916 (2013).
24. Capolicchio, S., Wang, H. C., Thakor, D. T., Shears, S. B. & Jessen, H. J. Synthesis of densely phosphorylated Bis-1,5-diphospho-myo-inositol tetrakisphosphate and its enantiomer by bidirectional P-anhydride formation. *Angew. Chem. Int. Ed.* **53**, 9508–9511 (2014).
25. Falck, J. R. *et al.* Synthesis and structure of cellular mediators—inositol polyphosphate diphosphates. *J. Am. Chem. Soc.* **117**, 12172–12175 (1995).
26. Laussmann, T., Reddy, K. M., Reddy, K. K., Falck, J. R. & Vogel, G. Diphospho-myo-inositol phosphates from Dictyostelium identified as D-6-diphospho-myo-inositol pentakisphosphate and D-5,6-bisdiphospho-myo-inositol tetrakisphosphate. *Biochem. J.* **322**, 31–33 (1997).
27. Reddy, K. M., Reddy, K. K. & Falck, J. R. Synthesis of 2- and 5-diphospho-myo-inositol pentakisphosphate (2- and 5-PP-InsP(5)), intracellular mediators. *Tetrahedron Lett.* **38**, 4951–4952 (1997).
28. Wang, H. C. *et al.* Synthetic inositol phosphate analogues reveal that PPIP5K2 has a surface-mounted substrate capture site that is a target for drug discovery. *Chem. Biol.* **21**, 689–699 (2014).
29. Wu, M., Dul, B. E., Trevisan, A. J. & Fiedler, D. Synthesis and characterization of non-hydrolysable diphosphoinositol polyphosphate messengers. *Chem. Sci.* **4**, 405–410 (2013).
30. Zhang, H., Thompson, J. & Prestwich, G. D. A scalable synthesis of the IP7Isomer, 5-PP-Ins(1,2,3,4,6)P5. *Org. Lett.* **11**, 1551–1554 (2009).
31. Watanabe, Y., Nakamura, T. & Mitsumoto, H. Protection of phosphate with the 9-fluorenylmethyl group. Synthesis of unsaturated-acyl phosphatidylinositol 4,5-bisphosphate. *Tetrahedron Lett.* **38**, 7407–7410 (1997).
32. Mentel, M., Laketa, V., Subramanian, D., Gillandt, H. & Schultz, C. Photoactivatable and cell-membrane-permeable phosphatidylinositol 3,4,5-trisphosphate. *Angew. Chem. Int. Ed.* **50**, 3811–3814 (2011).
33. Subramanian, D. *et al.* Activation of membrane-permeant caged PtdIns(3)P induces endosomal fusion in cells. *Nat. Chem. Biol.* **6**, 324–326 (2010).
34. Jessen, H. J., Schulz, T., Balzarini, J. & Meier, C. Bioreversible protection of nucleoside diphosphates. *Angew. Chem. Int. Ed.* **47**, 8719–8722 (2008).
35. Thomson, W. *et al.* Synthesis, bioactivation and anti-hiv activity of the Bis (4-Acyloxybenzyl) and Mono(4-Acyloxybenzyl) esters of the 5'-monophosphate of Azt. *J. Chem. Soc. Perkin Trans. 1*, 1239–1245 (1993).
36. Cremonnik, G. S., Hofer, A. & Jessen, H. J. Iterative synthesis of nucleoside oligophosphates with phosphoramidites. *Angew. Chem. Int. Ed.* **53**, 286–289 (2014).
37. Hofer, A. *et al.* A Modular synthesis of modified phosphoanhydrides. *Chem. Eur. J.* **21**, 10116–10122 (2015).
38. Losito, O., Szigyarto, Z., Resnick, A. C. & Saiardi, A. Inositol pyrophosphates and their unique metabolic complexity: analysis by gel electrophoresis. *PLoS ONE* **4**, e5580 (2009).
39. Anstaett, P., Leonidova, A. & Gasser, G. Caged phosphate and the slips and misses in determination of quantum yields for ultraviolet-A-induced photouncaging. *ChemPhysChem* **16**, 1857–1860 (2015).
40. Anstaett, P., Leonidova, A., Janett, E., Bochet, C. G. & Gasser, G. Reply to commentary by trentham *et al.* on "caged phosphate and the slips and misses in determination of quantum yields for ultraviolet-a-induced photouncaging" by Gasser *et al.* *ChemPhysChem* **16**, 1863–1866 (2015).
41. Corrie, J. E., Kaplan, J. H., Forbush, B., Ogdren, D. C. & Trentham, D. R. Commentary on "caged phosphate and the slips and misses in determination of quantum yields for ultraviolet-a-induced photouncaging" by G. Gasser and Co-Workers. *ChemPhysChem* **16**, 1861–1862 (2015).
42. Schonleber, R. O., Bendig, J., Hagen, V. & Giese, B. Rapid photolytic release of cytidine 5-diphosphate from a coumarin derivative: A new tool for the investigation of ribonucleotide reductases. *Bioorg. Med. Chem.* **10**, 97–101 (2002).
43. Stanzl, E. G., Trantow, B. M., Vargas, J. R. & Wender, P. A. Fifteen years of cell-penetrating guanidinium-rich molecular transporters: basic science, research tools, and clinical applications. *Acc. Chem. Res.* **46**, 2944–2954 (2013).
44. Lee, H. L. *et al.* Single-molecule motions of oligoarginine transporter conjugates on the plasma membrane of Chinese hamster ovary cells. *J. Am. Chem. Soc.* **130**, 9364–9370 (2008).
45. Rothbard, J. B., Jessop, T. C., Lewis, R. S., Murray, B. A. & Wender, P. A. Role of membrane potential and hydrogen bonding in the mechanism of translocation of guanidinium-rich peptides into cells. *J. Am. Chem. Soc.* **126**, 9506–9507 (2004).
46. Wender, P. A., Galliher, W. C., Goun, E. A., Jones, L. R. & Pillow, T. H. The design of guanidinium-rich transporters and their internalization mechanisms. *Adv. Drug Deliv. Rev.* **60**, 452–472 (2008).
47. Wilson, M. S. C., Bulley, S. J., Pisani, F., Irvine, R. F. & Saiardi, A. A novel method for the purification of inositol phosphates from biological samples reveals that no phytate is present in human plasma or urine. *Open Biol.* **5**, 150014 (2015).
48. Cormack, B. P., Valdivia, R. H. & Falkow, S. FACS-optimized mutants of the green fluorescent protein (GFP). *Gene* **173**, 33–38 (1996).
49. Laketa, V. *et al.* PIP(3) induces the recycling of receptor tyrosine kinases. *Sci. Signal.* **7**, ra5 (2014).
50. Jo, H. *et al.* Small molecule-induced cytosolic activation of protein kinase Akt rescues ischemia-elicited neuronal death. *Proc. Natl Acad. Sci. USA* **109**, 10581–10586 (2012).
51. Lemmon, M. A. Pleckstrin homology (PH) domains and phosphoinositides. *Biochem. Soc. Symp.* **74**, 81–93 (2007).
52. Schindelin, J. *et al.* Fiji: an open-source platform for biological-image analysis. *Nat. Methods* **9**, 676–682 (2012).

Acknowledgements

Imaging was performed with support of the Center for Microscopy and Image Analysis at UZH and the Stanford Shared FACS Facility. We thank Professors Jay Siegel, John Robinson, Adolfo Saiardi, Robert Waymouth, Chris Contag, Lynette Cegelski, Dr. Vanessa Pierroz, Dr. Riccardo Rubbiani and Dr. Vibor Laketa for discussions, materials and procedures. This work was supported by The Swiss National Science Foundation (PP00P2_157607 to H.J.J. and PP00P2_133568 & PP00P2_157545 to G.G.), the National Institutes of Health (NIH-CA031841, NIH-S10RR027431-01 and NIH-CA031845 to P.A.W.), and the Deutsche Forschungsgemeinschaft (DFG, TRR83 to C.S.). Fellowships: National Science Foundation and the Stanford Center for Molecular Analysis and Design.

Author contributions

I.P., D.T.T., R.C.C., J.R.V., C.J.M., P.A. and S.H. conducted the experiments. H.J.J., P.A.W., C.S., L.B. and G.G. planned the experiments. H.J.J., P.A.W., J.R.V. and C.J.M. wrote the manuscript. All authors discussed the results and revised the manuscript.

Additional information

Supplementary Information accompanies this paper at <http://www.nature.com/naturecommunications>

Competing financial interests: The authors declare no competing financial interests.

Reprints and permission information is available online at <http://npng.nature.com/reprintsandpermissions/>

How to cite this article: Pavlovic, I. *et al.* Cellular delivery and photochemical release of a caged inositol-pyrophosphate induces PH-domain translocation in *cellulo*. *Nat. Commun.* **7**:10622 doi: 10.1038/ncomms10622 (2016).



This work is licensed under a Creative Commons Attribution 4.0 International License. The images or other third party material in this article are included in the article's Creative Commons license, unless indicated otherwise in the credit line; if the material is not included under the Creative Commons license, users will need to obtain permission from the license holder to reproduce the material. To view a copy of this license, visit <http://creativecommons.org/licenses/by/4.0/>